Improved Dual-Level Direct Dynamics Method for Reaction Rate Calculations with Inclusion of Multidimensional Tunneling Effects and Validation for the Reaction of H with *trans*-N_2H_2

Yao-Yuan Chuang and Donald G. Truhlar*

Department of Chemistry and Supercomputer Institute, University of Minnesota, Minneapolis, Minnesota 55455-0431

Received: December 20, 1996; In Final Form: February 28, 1997[⊗]

A new scheme for carrying out dual-level direct dynamics calculations is presented in this paper. A better estimate of the barrier width is obtained by using the high-level imaginary frequency at the saddle point as well as high-level values of the energies of three stationary points (i.e., reactants, products, and saddle point). Furthermore, a more robust formula is introduced for incorporating high-level vibrational frequency corrections on the generalized normal modes along the reaction path. Incorporating these improvements, we carry out dual-level calculations of the reaction rate of H + N_2H_2 → H_2 + N_2H by employing variational transition-state theory with optimized multidimensional tunneling. Dual-level calculations at the level of zero-curvature tunneling (ZCT) show excellent agreement with an earlier calculation involving high-level computations at 11 times as many geometries. Having validated the dual-level approach at the ZCT level, we next extend the dual-level calculations to include small-curvature, large-curvature, and optimized multidimensional tunneling approximations. Four choices of low-level surface are used to gauge the sensitivity to these choices.

1. Introduction

Direct dynamics calculations, that is, the calculation of rate coefficients or other dynamical information directly from electronic structure calculations without the intermediacy of fitting an analytic potential energy function, provide one of the most promising current avenues of approach in theoretical chemical kinetics.[1] In our opinion, the fast lane on this avenue is dual-level direct dynamics.[2−5] Our approach to dual-level direct dynamics involves the simultaneous use of two levels of electronic structure theory: a "low level" that is used at a large number of geometries and a "high level" which is required only at a few selected points. In most work carried out so far, these points are selected to be the reactants, products, and saddle point and possibly a precursor and/or successor complex.[2−5] (One attempt at developing dual-level methods with a more general situation of low-level points has been reported as well.[6]) The low level may be an *ab initio* level,[3] e.g., MP2/6-31G(*d*,*p*),[7] a generally parametrized semiempirical method,[2] e.g., MNDO,[8] AM1,[9] or PM3,[10] or a semiempirical method with specific reaction parameters,[2−5] e.g., NDDO-SRP.[11−13] (Specific reaction parameters may also be developed for a range of systems, still, however, more restricted than in the general parametrizations; in such cases they have also been called specific-range parameters, again abbreviated SRP,[14] or system-specific parameters, abbreviated SSP.[15])

In the present paper we present two improvements in the dual-level direct dynamics method, and we apply the improved algorithm with AM1, MNDO, and NDDO-SRP methods to the reaction of H with *trans*-diazene (N_2H_2). First of all, comparing our results to the extensive high-level calculations of Linder *et al*.[16] allows us to test and validate the dual-level approach at the zero-curvature-tunneling dynamical level. Second, the dual-level approach allows us to include more reliable tunneling estimates than are available from the previous single-level calculations.

The H + N_2H_2 reaction is 40 kcal exothermic because the N−H bond is very weak, and thus the reaction is important for combustion and pyrolysis mechanisms of nitrogen-containing substances, such as ammonia.

2. Methods

2.1. Dynamical Theory. We employ canonical variational transition-state theory (CVT) with a transmission coefficient calculated by the microcanonical optimized multidimensional tunneling approximation (μOMT).

The CVT method[17−19] involves calculating the generalized transition-state (GT) free energy of the activation profile defined by[17−21]

$$\Delta G_T^{\mathrm{GT},\circ} = RT \ln\left(\frac{Q^{\mathrm{GT}}(T,s)K^\circ}{\Phi^{\mathrm{R}}(T)}\right) \qquad (1)$$

where T is temperature, R is the gas constant, $Q^{\mathrm{GT}}(T,s)$ is a partition function for a generalized transition state located a signed distance s along the minimum-energy path[21,22] (MEP) from the saddle point, K° is the reciprocal of the standard-state concentration, and $\Phi^{\mathrm{R}}(T)$ is the reactant partition function per unit volume. In eq 1, $Q^{\mathrm{GT}}(T,s)$ contains the reaction path symmetry factor σ. Then the variational transition state is optimized by finding the value $s = s_*(T)$ at which $\Delta G_T^{\mathrm{GT},\circ}$ is a maximum, and the CVT rate coefficient is given by

$$k^{\mathrm{CVT}}(T) = \frac{k_{\mathrm{B}}T}{h}K^\circ \exp\{-\Delta G_T^{\mathrm{GT},\circ}[T,s_*(T)]/RT\} \qquad (2)$$

where k_{B} is Boltzmann's constant and h is Planck's constant.

Tunneling effects are included by factoring in a ground-state transmission coefficient[19−21] $\kappa^{\mathrm{tun}}(T)$, i.e.,

$$k^{\mathrm{CVT/tun}}(T) = \kappa^{\mathrm{tun}}(T)\, k^{\mathrm{CVT}}(T) \qquad (3)$$

where

[⊗] Abstract published in *Advance ACS Abstracts,* April 15, 1997.

S1089-5639(97)00052-2 CCC: $14.00

$$\kappa^{\mathrm{tun}}(T) = \frac{\int \mathrm{d}E\, P^{\mathrm{G}}(E)\, \mathrm{e}^{-E/RT}}{\int \mathrm{d}E\, \theta(E - V_{\mathrm{a}}^{\mathrm{G}*})\, \mathrm{e}^{-E/RT}} \quad (4)$$

$$V_{\mathrm{a}}^{\mathrm{G}*}(T) = V_{\mathrm{a}}^{\mathrm{G}}[s_*(T)] \quad (5)$$

$$V_{\mathrm{a}}^{\mathrm{G}}(s) = V_{\mathrm{MEP}}(s) + \epsilon_{\mathrm{vib}}^{\mathrm{G}}(s) \quad (6)$$

E is total energy, $P^{\mathrm{G}}(E)$ is the probability for a system with energy E to be transmitted through the ground-state level of the transition state, $\theta(x)$ is a unit step function at $x = 0$, $V_{\mathrm{MEP}}(s)$ is the Born−Oppenheimer potential energy along the MEP at s, and $\epsilon_{\mathrm{vib}}^{\mathrm{G}}(s)$ is the ground-state vibrational energy, excluding reaction-coordinate motion, at s. We consider four methods for approximating $P^{\mathrm{G}}(E)$:

ZCT	zero-curvature tunneling,[19,22] in which $P^{\mathrm{G}}(E)$ is the transmission probability for $V_{\mathrm{a}}^{\mathrm{G}}(s)$ ignoring reaction-path curvature
SCT	small-curvature tunneling, in which $P^{\mathrm{G}}(E)$ is approximated by the centrifugal-dominant small-curvature semiclassical adiabatic ground-state method[23,24] (CD-SCSAG), yielding $P^{\mathrm{SCT}}(E)$
LCT	large-curvature tunneling, in which $P^{\mathrm{G}}(E)$ is approximated by the large-curvature ground-state method, version 3[12,21,23,25,26] (LCG3), yielding $P^{\mathrm{LCT}}(E)$
μOMT	microcanonical optimized multidimensional tunneling,[27,28] in which $P^{\mu\mathrm{OMT}}(E) = \max[P^{\mathrm{SCT}}(E), P^{\mathrm{LCT}}(E)]$

The SCT method is expected to be accurate when the curvature of the MEP is small between the tunneling turning points, and $P^{\mathrm{LCT}}(E)$ is expected to be accurate when the curvature is large. Both methods are expected to underestimate the tunneling probability when used out of their regime of validity; this motivates $P^{\mu\mathrm{OMT}}(E)$. In our experience, based on cases where we have calculations by the more general least-action semiclassical method or by accurate quantum mechanical scattering theory available for comparison, the use of $P^{\mu\mathrm{OMT}}(T)$ appears to be adequate for general use.[28−31]

In the present paper, rotations are treated by the classical rigid-rotator approximation and vibrations are treated as quantum mechanical harmonic oscillators, with the generalized normal modes defined in rectilinear coordinates. With these approximations the system properties required for the various levels of dynamical calculations are as follows:

CVT	reactant geometry, energy, and vibrational frequencies ω_m^{R} and generalized-transition-state geometries, energies, and vibrational frequencies $\omega_m^{\mathrm{GT}}(s)$, where $m = 1, 2, \ldots$ labels the vibrational modes (note: the saddle point properties are included since the saddle point is a generalized transition state with $s = 0$)
CVT/ZCT	same requirements as CVT
CVT/SCT	same requirements as CVT and CVT/ZCT
CVT/LCT	same as CVT/SCT plus generalized normal mode eigenvectors and energies at regularly spaced points along energy-dependent large-curvature tunneling paths through the reaction swath (the reaction swath is a union of the small-curvature reaction valley near the reaction path and the wider region traversed by large-curvature tunneling paths[32,33])

The next subsection describes a dual-level scheme for obtaining all of this information from electronic structure calculations.

2.2. Interface of Dynamics and Electronic Structure. In the dual-level approach that we have developed,[2] all reactant properties and saddle point properties other than geometry are obtained at the high level, geometries of generalized transition states and large-curvature tunneling paths are obtained at the low level, and properties other than geometry for generalized transition states with $s \neq 0$ and for tunneling points in the swath are obtained by "correcting" low-level calculations. Corrections are also applied to moments of inertia. The corrections are all based on interpolation of the deviations between high-level (HL) calculations for the saddle point, reactants, and products and low-level (LL) calculations for the same three stationary points. (For the choices of high level and low level for the present calculation, see section 3; this section is more general.) Methods that can be used for these corrections are fully explained elsewhere,[2] and they can be illustrated by considering the vibrational frequencies, as we do next. Another motivation for reviewing the treatment of the vibrational frequencies in this paper is that we present an improvement in the way this particular correction is handled.

Let $\omega_m^{\mathrm{LL}}(s)$, $m = 1, 2, \ldots, F - 1$ (where $F = 3N - 6$ for an N-atom nonlinear generalized transition state) denote the low-lying frequencies of the generalized transition state at s. The frequencies are numbered by arranging them in decreasing order. In the original method,[2] which will be called "interpolated corrections—additive" (ICA) in the present paper, the dual-level (i.e., DL or corrected) frequencies were given by

$$\omega_m^{\mathrm{DL}}(s) = \omega_{\mathrm{m}}^{\mathrm{LL}}(s) + f^{\mathrm{ICA}}(s) \quad (7)$$

where

$$f^{\mathrm{ICA}}(s) = \mathrm{interpolant}\{\, \omega_{\mathrm{m}}^{\mathrm{HL}}(s) - \omega_{\mathrm{m}}^{\mathrm{LL}}(s)\}_{s=-\infty,0,+\infty} \quad (8)$$

The meaning of eq 8 is that $f^{\mathrm{ICA}}(s)$ is interpolated from three values (in the present case: reactants, $s = -\infty$; saddle point, $s = 0$; and product, $s = +\infty$) of the difference of high-level and low-level frequencies. Note that the HL frequencies, like the LL ones, are arranged in decreasing order. For further discussion we define a sign-conserving interpolant as one that has the following property: If all of the data to be interpolated have the same sign, the interpolant preserves that sign at all values of s. Although it is not necessary for us to repeat all the details of our interpolants[2] in the present paper, we note that they are all sign preserving.

Although the ICA method has generally been successful, it has one disadvantage, namely, even when all values of $\omega_m^{\mathrm{LL}}(s)$ and $\omega_m^{\mathrm{HL}}(s)$ are real and positive for $s = -\infty$, 0, and $+\infty$ and even when the interpolant has the property that it is sign preserving, the above scheme can still yield $\omega_m^{\mathrm{DL}}(s)$ values that are negative, which makes no sense. (Due to the unfortunate circumstance that many electronic structure programs print out imaginary frequencies as negative numbers, we have noticed much confusion between negative and imaginary frequencies, so we emphasize here that we do mean negative, not imaginary.)

To eliminate the negative-frequency problem, we propose an alternative method, called "interpolated corrections based on the logarithm" (ICL). This method is defined by

$$\omega_m^{\mathrm{DL}}(s) = \omega_m^{\mathrm{LL}}(x)\, \exp[f^{\mathrm{ICL}}(s)] \quad (9)$$

where

$$f^{\mathrm{ICL}}(s) = \mathrm{interpolant}\{\ln[\omega m^{\mathrm{HL}}(s)/\omega_m^{\mathrm{LL}}(s)]\}_{s=-\infty,0+\infty} \quad (10)$$

We use the same interpolating functions in eq 10 as those presented previously[2] for eq 8. These interpolating functions are sign preserving. Then, with the ICL scheme (but not the ICA scheme), $\omega_m^{\mathrm{DL}}(s)$ must be positive. Looking to possible future developments, the logarithm scheme is more robust than simply using the ratio without the logarithm in eq 10 because

it guarantees positive values of $\omega_m^{DL}(s)$ even with more general interpolating schemes (e.g., products of polynomials and exponential functions) that are not sign preserving.

A second improvement in the original algorithm[2] concerns the interpolated corrections for $V_{MEP}(s)$. Originally, we obtained the dual-level potential curve along the MEP by

$$V_{MEP}^{DL}(s) = V_{MEP}^{LL}(s) + \text{interpolant}\{V_{MEP}^{HL}(s) - V_{MEP}^{LL}(s)\} \quad (11)$$

where the interpolant is again based on values of the function interpolated at three stationary points. We have found that the chief source of inaccuracy in the original method is its inability to sufficiently improve the low-level barrier shape, especially its width. The barrier height is corrected with the original interpolated correction method, but the barrier width is typically very similar to that on the low-level surface.

Since our algorithm assumes that a high-level Hessian is available at the saddle point, one can in principle use the high-level imaginary frequency at the saddle point to improve the shape of $V_{MEP}(s)$ in the vicinity of its maximum, but the imaginary frequency information was not used for this purpose in the original algorithm. The modification introduced here corrects this. In particular, in this paper, global Eckart functions[34] are used to fit three stationary-point energies and the saddle point imaginary frequency at the high level and to fit energies at four points (reactants, products, saddle point, and one extra point) on the low-level MEP. The improved dual-level $V_{MEP}(s)$ value is then defined as

$$V_{MEP}^{DL}(s) = V_{MEP}^{LL}(s) + [V_{Eck}^{HL}(s) - V_{Eck}^{LL}(s)] \quad (12)$$

where

$$V_{Eck}(s) = \frac{AY}{1+Y} + \frac{BY}{(1+Y)^2} + C \quad (13)$$

$$Y = \exp\left(\frac{s - S_0}{L}\right) \quad (14)$$

$$A = V_{MEP}(s = +\infty) - V_{MEP}(s = -\infty) \quad (15)$$

$$C = V_{MEP}(s = -\infty) \quad (16)$$

$$B = (2V^{\ddagger} - A - 2C) \pm 2[(V^{\ddagger} - C)(V^{\ddagger} - A - C)]^{1/2} \quad (17)$$

$$S_0 = -L \ln\left(\frac{A+B}{B-A}\right) \quad (18)$$

$V^{\ddagger}$ is the classical barrier height, μ is the scaling mass[21] (set equal to 1.0 amu in the present study), and L is a range parameter. The range parameter for V_{Eck}^{HL} is obtained by

$$L^{HL} = \left[-\frac{2V^{\ddagger}(V^{\ddagger} - A)}{\mu(\omega^{\ddagger})^2 B}\right]^{1/2} \quad (19)$$

in terms of the high-level imaginary frequency ($\omega^{\ddagger}$). For the low-level surface we have more global information available on the shape of the barrier, and we use it. Note that eqs 16−18 force the Eckart fit to pass through the reactant, product, and saddle point values of $V_{MEP}(s)$ and to have a maximum at $s = 0$. Then, L for the $V_{MEP}^{LL}(s)$ is determined such that the Eckart fit to $V_{MEP}(s)$ agrees with it not only at the three stationary points but also at a fourth point located a finite distance away from the saddle point. This extra point is located on the high-energy side of the saddle point, that is, at $s > 0$ if the product-side stationary point is higher in energy than the reactant-side stationary point and $s < 0$ otherwise. Furthermore, we take this point half-way down in energy from the saddle point to the reactant-side or product-side stationary point, whichever is higher. (It is important, in our opinion, to define fitting choices clearly and stay the course with them; we can only validate a method and build up experience with it if the algorithm is well-defined and used in a consistent fashion.)

We note that corrections to the barrier shape off the MEP (i.e., in the swath where large-curvature tunneling[21,23,25−27] occurs) are obtained[2] from the corrections on the MEP, so this procedure effectively corrects the barrier shape for corner-cutting tunneling as well as for tunneling along the MEP.

No change is made in the correction scheme for the determinant of the moment of inertia.

TABLE 1: Semiempirical Parameters Adjusted in SRP Models[a]

	MNDO-SRP		AM1-SRP	
	value	change (%)	value	change (%)
U_{ss}(N)	−69.932 122	3		
U_{pp}(N)	−51.872 319	9	−52.330 81	8
β_p(N)	−18.495 758	10		
β_s(H)	−7.315 906 4	5	−5.708 1	8

[a] Notation and units are the same as in original ref 8 and 9.

3. Computational Details

The HL properties for $s = -\infty$, 0, and $+\infty$ were taken from the published work of Linder *et al.*[16] They used the complete-active-space self-consistent-field (CASSCF) method with the correlation-consistent polarized valence double ζ basis set[35] to optimize geometries of the stationary points and to calculate vibrational frequencies, and they used multireference configuration interaction (MRCI) at the CASSCF geometries to calculate the energies at the stationary points. They reported MRCI calculations for more than one one-electron basis set and more than one configuration list; the ones used here are based on their best calculations, denoted[16] MRCI/cc-pVTZ.

The LL calculations were calculated by the MNDO[8] and AM1[9] methods and by two NDDO-SRP parametrizations developed specifically for this work. The NDDO-SRP parameters were adjusted by trial and error to give reasonably accurate (where "accurate" is defined by the Linder *et al*. HL calculations) values of $V_a^G(s = 0)$, the saddle point geometry, and the exoergicity and are presented in Table 1. Ideally, this step would be carried out in a systematic, mathematically justified manner. However, at present, adjustment of SRP parameters is still somewhat of an art, and the justification for accepting a particular low-level surface as "reasonable" is based on physical considerations. In particular we believe that a low-level surface should, if possible, be approximately correct for at least the saddle point geometry and energy, and preferably it should also be approximately correct for the exoergicity, the vibrational frequencies, and the barrier width. Since the effects of errors in these quantities propagate in a nonlinear fashion, we will carry out full rate-coefficient calculations with more than one choice for the low-level implicit surface as a way to gauge the effect of the choice of low-level surface on the final results.

All dynamics calculations were carried out using a locally modified version of the MORATE program.[26,36] Geometry optimizations were carried out by using MOPAC[37] enhanced locally by the addition of the eigenvector following (EF) algorithm.[38] The reaction path was followed using the Page−McIver[39] method with a gradient step size of 0.01 a_0 and a Hessian step size of 0.01 a_0 for AM1 and AM1-SRP and

TABLE 2: Bond Energies, Saddle Point Properties, and Energy of Reaction for H(1) + H(2)−N−N−H(3) → H(1)−H(2) + N−N−H(3)

quantity	explanation	G2	MRCI//CASSCF	MNDO	AM1	MNDO-SRP	AM1-SRP
			Bond Energies				
H−H	D_e	110.3		103.4	109.4	113.8	94.0
H−N	D_e	73.8		65.1	61.9	70.3	62.5
			Overall Reaction Energetics				
ΔE	*a*	−36.5	−33.6	−38.4	−47.5	−43.5	−31.6
$\Delta H_0°$	*b*	−40.3	−37.4	−41.9	−50.4	−46.6	−35.3
			Transition-State Properties				
$V^{\ddagger}$	*c*		5.9	15.0	4.3	6.7	6.2
$\Delta V_a^{\ddagger G}$	*d*		4.3	12.9	2.8	4.3	4.3
H(1)−H(2)	*e*		1.20	0.97	1.06	1.00	0.96
H(2)−N	*e*		1.16	1.18	1.10	1.19	1.22
N−N	*e*		1.25	1.21	1.21	1.28	1.23
N−H(3)	*e*		1.06	1.03	1.02	1.06	1.07
H(1)−H(2)−N	*f*		173.5	179.6	178.7	179.4	179.7
H(2)−N−N	*f*		106	112	112	105	105
N−N−H(3)	*f*		106	113	113	103	104

[a] Energy of reaction, excluding zero-point energy, kilocalories. [b] Energy of reaction including zero-point energy, kilocalories. [c] Classical barrier height, kilocalories. [d] Zero-point-corrected barrier height, kilocalories. [e] Bond distance, Angstroms. [f] Bond angle, degrees.

gradient and Hessian step sizes of 0.02 a_0 for MNDO and MNDO-SRP. Reaction path information was saved on the Hessian grid and was interpolated to the variational transition state by three- and five-point Lagrangian interpolation. Quadratures involved in the tunneling calculations were carried out with 30 coordinate points for each action integral and were Boltzmann averaged using 30 energies.

The symmetry number of the forward reaction is 2. All vibrational modes were treated as quantized harmonic oscillators in rectilinear coordinates.[21] Overall rotation was treated as separable and classical.

The L parameter used for $V_{MEP}^{LL}(s)$ calculations is 0.36 a_0 for AM1, 0.32 a_0 for AM1-SRP, 0.36 a_0 for MNDO, and 0.54 a_0 for MNDO-SRP. The L^{HL} value calculated from the imaginary frequency at the high level is 0.225 a_0 with a barrier height of 5.91 kcal/mol and an exothermicity of −33.63 kcal/mol.

4. Results

Table 2 compares the transition-state and reaction properties obtained by two standard NDDO (neglect of diatomic differential overlap) semiempirical methods, MNDO and AM1, to two sets of high-level results, the Gaussian-2 (G2) calculations of Pople and Curtiss,[40] which are available only for reactants and products, and the MRCI calculations of Linder *et al.*,[16] which are based on geometries and Hessians optimized at the CASSCF level. (Zero-point energies were also evaluated[16] at the CASSCF level.)

All methods in Table 2 agree that the reaction is very exothermic with an early transition state. The zero-point-corrected barrier heights show deviations of 1.5−8.6 kcal from the MRCI values, the bond distances of the making bond show deviations of 0.14−0.23 Å, and the N−N−H bond angles show deviations of 6−7 degrees. Next we adjusted some of the NDDO parameters to improve the agreement with the MRCI values for these quantities and for the frequencies. Following our usual practice, we arbitrarily restricted all parameter changes to 10% or less because we believe that keeping the parameters within this range of the widely validated general parametrization makes it less likely that the implicit low-level surface will have qualitatively incorrect features. The adjusted parameters are shown in Table 1, and the modified predictions are shown in the last two columns of Table 2. These modified methods are labeled SRP (specific reaction parameters) to denote that the parameters are adjusted to make the predictions more reliable for a specific reaction. In adjusting the parameters we especially focused on the zero-point-corrected barriers, which now show deviations of less than 0.1 kcal. Simultaneously the N−N−H bond angles are considerably improved, but the bond distance of the making bond proved difficult to adjust.

TABLE 3: Saddle Point Harmonic Frequencies

mode	CASSCF	MNDO	AM1	MNDO-SRP	AM1-SRP
1	3064	3381	3282	3133	2937
2	1607	2136	2175	1553	2042
3	1506	1562	1732	1463	1470
4	1328	1444	1502	1339	1399
5	1261	1191	1201	1179	1106
6	1214	1113	1172	988	1041
7	537	552	454	499	508
8	373	423	355	397	413
s	2391*i*	3192*i*	1446*i*	2039*i*	2291*i*
MAD[a]	0	228	259	100	130

[a] Mean absolute deviation from CASSCF values.

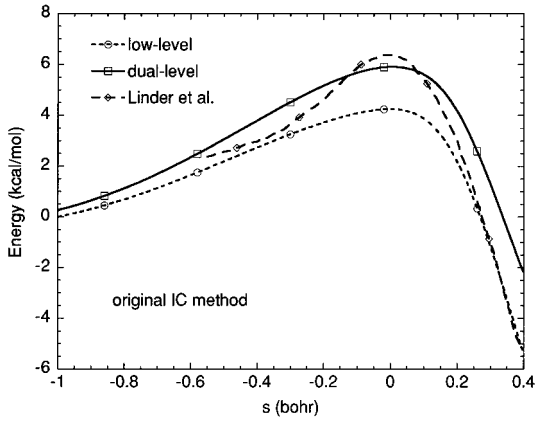

Figure 1. $V_{MEP}(s)$ at low level, high level, and dual level based on original dual-level scheme with AM1 as low-level surface.

Table 3 shows the harmonic vibrational frequencies at the saddle point. This table shows that we were able to reduce the mean value of the absolute deviation of the MNDO and AM1 frequencies from the CASSCF ones by factors of 2.3 and 2.0, respectively.

As an example, Figures 1 and 2 show the $V_{MEP}(s)$ curves of the dual-level calculations based on AM1. The short-dashed curves represent the low-level values from AM1, and the long-dashed curves correspond to the high-level results from Linder *et al.* (Ideally we would have plotted $V_{MEP}(s)$ from their

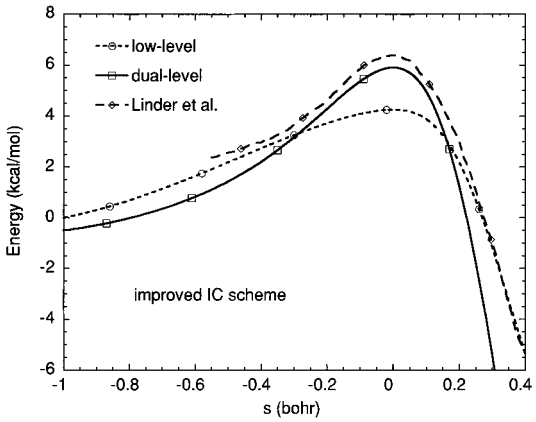

Figure 2. $V_{MEP}(s)$ at low level, high level, and dual level based on improved scheme of dual-level calculations incorporating Eckart barrier fits with AM1 as low-level surface.

MRCI55/cc-pVTZ calculation, which is their best calculation and is the one we used in eqs 11−19. However, that is not available as a function of reaction coordinate, so we plotted their MRCI33/m-pVTZ curve. However, the shape of $V_{MEP}(s)$ in their calculations is very similar[16] for all m-cc-pVTZ and cc-pVTZ levels.) The solid curve in Figure 1 is the dual-level result from the original scheme of eq 11, and the solid curve in Figure 2 is based on interpolated corrections with the new Eckart correction scheme of eqs 12−19. Clearly the high-level calculations of Linder *et al*. predict a narrower barrier than the AM1 calculations do. The original correction scheme in Figure 1 improves the barrier height, but still predicts too wide a barrier. The new correction scheme in Figure 2 improves the shape of the barrier quite dramatically. Note that the high-level results in Figures 1 and 2 are based on high-level points all along the reaction path, whereas the dual-level ones are based on low-level calculations along the reaction path with corrections based on high-level data from only three stationary points.

Table 4 gives calculated CVT/ZCT rate coefficients calculated in several different ways:

HL	high-level, which are the single-level direct dynamics calculations of Linder *et al*. based on CASSCF geometries gradients, and Hessians and MRCI energies at 33 points along the reaction path, including reactants, saddle point, and products
LL	low-level, which are single-level direct dynamics calculations at four different levels, MNDO, AM1, MNDO-SRP, and AM1-SRP
HL///LL	dual-level direct dynamics calculations, which are based on HL calculations at reactants, saddle point, and products only plus a full LL calculation
IVTST-0	interpolated variational transition state theory[41] based on HL calculations only at reactants, saddle points, and product

Corrections to the LL moments of inertia are evaluated at the three stationary points and interpolated by methods explained previously.[2] Corrections to LL vibrational frequencies are also evaluated at three points and are interpolated by the ICL method explained in section 2. The Eckart fit method was used to interpolate corrections to $V_{MEP}(s)$.

Table 4 shows that the results obtained using SRP low levels or interpolated corrections or both are uniformly accurate within 20−40% on average, although deviations from the full HL calculation may be higher at the lower end of the temperature range. (Results at the lowest temperatures are the most sensitive to the calculation of tunneling effects, and this part of the calculation is very sensitive to the estimation of barrier width, which can depend strongly on the choice of low level.) Results

TABLE 4: CVT/ZCT Rate Coefficients (cm^3 molecule^{-1} s^{-1})

			LL above HL///LL[b]				
T (K)	power of 10[a]	HL	MNDO	AM1	MNDO-SRP	AM1-SRP	IVTST-0
300	−13	6.8	0.00006	9.5	0.9	2.2	
			6.5	8.8	12	5.0	5.0
600	−12	3.5	0.005	5.3	1.7	2.3	
			3.9	3.5	4.1	3.2	3.2
1500	−11	3.4	0.2	4.5	3.3	3.7	
			3.7	3.5	3.5	3.8	4.3
3000	−10	2.0	0.4	1.8	2.0	2.1	
			1.8	1.7	1.7	1.8	2.4
MUPD[c]		0	93	30	30	24	
			8	9	24	21	21
MUDL[d]		0	1.94	0.10	0.22	0.13	
			0.03	0.04	0.08	0.08	0.08

[a] Power of 10; for all rate coefficients at this temperature, power of 10 is the same. [b] Upper entry, LL; lower entry, HL///LLL, where LL is MNDO, AM1, MNDO-SRP, or AM1-SRP. [c] Mean unsigned percentage deviation (average over eight temperatures). [d] Mean unsigned deviation of logarithm (average over eight temperatures).

obtained with a generally parametrized semiempirical method without SRP or IC are much less reliable than those obtained with SRP or IC, as illustrated by the single-level MNDO results. For the present reaction the AM1 results are fortuitously reasonable, but in general one would not expect the general parametrizations to perform as well as SRP ones.

To quantify the validation suite, average absolute error criteria were calculated. First we computed the mean unsigned percentage deviation, abbreviated MUPD, for each calculation X (e.g., X ≡ MNDO-IC, where IC denotes that interpolated corrections are employed, i.e., that the dual-level approach is used). This is defined by

$$\mathrm{MUPD} = \frac{100}{8}\sum_{i=1}^{8}\frac{|k_{\mathrm{X}}^{\mathrm{CVT/ZCT}}(T_i) - k_{\mathrm{HL}}^{\mathrm{CVT/ZCT}}(T_i)|}{k_{\mathrm{HL}}^{\mathrm{CVT/ZCT}}(T_i)} \quad (20)$$

where T_i is one of eight temperatures (300, 400, 600, 1000, 1500, 2000, 2400, and 3000 K) where we can compare to full HL calculation by Linder *et al*. We also computed the mean of the unsigned difference in logarithm, abbreviated MUDL, for each X, which is defined by

$$\mathrm{MUPD} = \frac{1}{8}\sum_{i=1}^{8}|\log_{10} k_{\mathrm{X}}^{\mathrm{CVT/ZCT}}(T_i) - \log_{10} k_{\mathrm{HL}}^{\mathrm{CVT/ZCT}}(T_i)| \quad (21)$$

where T_i is one of the same eight temperatures. These average errors are given in the last two rows of Table 4. The low-level methods without correction give mean unsigned deviations in $\log_{10} k(T)$ of 0.10−1.94, and employing interpolated corrections reduces these values to the range 0.03−0.08. Of course the improvement is most dramatic when the low-level result is inaccurate, but it is encouraging that when the low-level results are better, the IC method still yields further improvement.

The IVTST-0 results are also encouragingly accurate. However, this method is less promising for general applications to systems where tunneling is important since one cannot (at least without fundamental changes in the character of the method) extend it to include SCT, LCT, or μOMT tunneling, whereas the dual-level methods can be and in fact have been so extended.

Table 5 provides another view of the results by concentrating on the transmission coefficient rather than the whole rate coefficient. Again we see improvement due to the corrections. For example, without corrections, the transmission coefficients at 300 K as computed from the various low-level potential

TABLE 5: $k^{CVT/ZCT}/k^{CVT}$ Ratios

		LL over HL///LL[a]				
T (K)	HL	MNDO	AM1	MNDO-SRP	AM1-SRP	IVTST-0
300	23	475	3.1	3.7	8.7	
		22	29	47	40	16
600	2.6	5.6	1.0	1.4	1.8	
		2.9	2.4	3.2	3.1	2.1
1500	1.2	1.3	0.8	1.0	1.1	
		1.2	1.0	1.1	1.2	1.1
3000	1.1	1.0	0.8	1.0	1.0	
		1.0	0.9	1.0	1.0	1.0

[a] Upper entry, LL; lower entry, HL///LL, where LL = MNDO, AM1, MNDO-SRP, or AM1-SRP.

TABLE 6: Rate Coefficients (cm^3 molecule^{-1} s^{-1}) by MRCI///AM1 Method

T (K)	power of 10[a]	CVT	CVT/SCT	CVT/LCT	CVT/μOMT
300	−12	0.03	3.8	1.1	3.8
400	−12	0.20	4.8	1.7	4.8
600	−12	1.5	7.8	3.7	7.8
1000	−11	1.0	1.9	1.3	1.9
1500	−11	3.4	4.3	3.6	4.3
2000	−11	7.3	7.7	6.9	7.7
2400	−10	1.1	1.1	1.1	1.1
3000	−10	1.9	1.8	1.7	1.8

[a] All entries for a given temperature are to be multiplied by this power of 10.

surfaces range from as low as 3 to as high as 475. The corrections considerably narrow the range of predictions to 22−47, as compared to the full high level value of 23 at 300 K. The narrowing and improvement of the range of prediction is still quite dramatic at 600 K.

Having established that the improved IC algorithm provides reasonably good agreement with full calculations at the CVT/ZCT level, we can then use these methods to calculate more accurate transmission coefficients that include reaction-path-curvature effects in the tunneling calculation. In particular we calculated the rate coefficients using the CVT/SCT, CVT/LCT, and CVT/μOMT levels of dynamical theory. The results are given in Table 6. We chose the AM1 method for this comparison because, of the four low levels tested, it gives the best saddle point geometry, and that is probably the single most desirable quality in a low-level method for the IC algorithm. Table 6 shows that small-curvature tunneling dominates large-curvature tunneling at essentially all energies and temperatures. Furthermore small-curvature tunneling is predicted to increase the rate coefficient (compared to zero-curvature tunneling) by factors of 4.3, 3.3, and 2.2 at 300, 400, and 600 K.

There is no experiment available for comparison, and the last column of Table 6, being the most complete calculation carried out to date, may be considered the most reliable available prediction. Of course there is still considerable room for improvement. Four areas for future work may be singled out in particular. First, none of the low-level surfaces is totally satisfactory from the point of view of saddle point geometry, and a better low-level surface would be very desirable. Second, one would expect smaller rates if the generalized normal modes were calculated in curvilinear coordinates.[42,43] Third, the effect of anharmonicity[20,44−47] should be examined. Fourth, it would be desirable to develop systematic extensions of the IC method allowing the convenient use of high-level data at additional points significantly removed from the saddle point. We hope to have the tools for at least some of these kinds of improvements in the near future.

5. Summary

We have presented a new interpolated correction method for dual-level direct dynamics calculations of rate coefficients by variational transition-state theory with multidimensional semiclassical tunneling contributions. The low-level potential energy along the minimum-energy path is corrected by adding the difference of two Eckart fits, where the high-level Eckart fit builds in information about the barrier width by using the high-level imaginary frequency at the saddle point. The frequencies along the reaction path are corrected by interpolating the logarithm of the ratio of the high-level and low-level values. The method is validated by comparing to the full high-level calculations of Linder *et al*. at the level of canonical variational theory with zero-curvature tunneling (CVT/ZCT). A critical point to emphasize is that we essentially reproduced the rate coefficients that they calculated based on a CASSCF reaction path and high-level energies at 33 points by using only the information in their published paper at three stationary points. Then the method is employed to estimate the effect of reaction-path curvature on the tunneling. Curvature effects are predicted to increase the reaction rate by a factor of 4 at 300 K.

Acknowledgment. This work was supported in part by the U. S. Department of Energy, Office of Basic Energy Sources.

References and Notes

(1) For a review of direct dynamics calculations, see: Truhlar, D. G. In *The Reaction Path in Chemistry: Current Approaches and Perspectives*; Heidrich, D., Ed.; Kluwer: Dordrecht, The Netherlands, 1995; pp 229−255.
(2) Hu, W.-P.; Liu, Y.-P.; Truhlar, D. G. *J. Chem. Soc., Faraday Trans.* **1994**, *90*, 1715.
(3) Corchado, J. C.; Espinosa-Garcia, J.; Hu, W.-P.; Rossi, I.; Truhlar, D. G. *J. Phys. Chem.* **1995**, *99*, 687.
(4) Hu, W.-P.; Truhlar, D. G. *J. Am. Chem. Soc.* **1995**, *117*, 10726.
(5) Hu, W.-P.; Truhlar, D. G. *J. Am. Chem. Soc.* **1996**, *118*, 860.
(6) Nguyen, K. A.; Rossi, I.; Truhlar, D. G. *J. Chem. Phys.* **1995**, *103*, 5522.
(7) Hehre, W. J.; Radom, L.; Schleyer, P. v. R.; Pople, J. A. *Ab Initio Molecular Orbital Theory*; Wiley: New York, 1986.
(8) Dewar, M. J. S.; Thiel, W. *J. Am. Chem. Soc.* **1977**, *99*, 4899.
(9) Dewar, M. J. S.; Zoebisch, E. G.; Healy, E. F.; Stewart, J. J. P. *J. Am. Chem. Soc.* **1985**, *107*, 3902.
(10) Stewart, J. J. P. *J. Comput. Chem.* **1989**, *10*, 221.
(11) Gonzalez-Lafont, A.; Truong, T. N.; Truhlar, D. G. *J. Phys. Chem.* **1991**, *95*, 4618.
(12) Liu, Y.-P.; Lu, D.-h.; Gonzalez-Lafont, A.; Truhlar, D. G.; Garrett, B. C. *J. Am. Chem. Soc.* **1993**, *115*, 7806.
(13) Rossi, I.; Truhlar, D. G. *Chem. Phys. Lett.* **1995**, *233*, 231.
(14) Barrows, S. E.; Dulles, F. J.; Cramer, C. J.; French, A. D.; Truhlar, D. G. *Carbohydr. Res.* **1995**, *276*, 219.
(15) Bash, P.; Ho, L. L.; Mackerell, A. D.; Levine, D.; Hallstrom, P. *Proc. Natl. Acad. Sci. U.S.A.* **1996**, *93*, 3698.
(16) Linder, D. P.; Duan, X.; Page, M. *J. Chem. Phys.* **1996**, *104*, 6298.
(17) Garrett, B. C.; Truhlar, D. G. *J. Chem. Phys.* **1979**, *70*, 1593.
(18) Garrett, B. C.; Truhlar, D. G. *J. Am. Chem. Soc.* **1979**, *101*, 4534.
(19) Garrett, B. C.; Truhlar, D. G.; Grev, R. S.; Magnuson, A. W. *J. Phys. Chem.* **1980**, *84*, 1730. Erratum: **1983**, *87*, 4554.
(20) Truhlar, D. G.; Isaacson, A. D.; Skodje, R. T.; Garrett, B. C. *J. Phys. Chem.* **1982**, *86*, 2252. Erratum: **1983**, *87*, 4554.
(21) Truhlar, D. G.; Isaacson, A. D.; Garrett, B. C. In *Theory of Chemical Reaction Dynamics*; Baer, M., Ed.; CRC Press: Boca Raton, FL, 1985; p 65.
(22) Truhlar, D. G.; Kuppermann, A. *J. Am. Chem. Soc.* **1971**, *93*, 1840.
(23) Lu, D.-h.; Truong, T. N.; Melissas, V. S.; Lynch, G. C.; Liu, Y.-P.; Garrett, B. C.; Steckler, R.; Isaacson, A. D.; Rai, S. N.; Hancock, G. C.; Lauderdale, J. G.; Joseph, T.; Truhlar, D. G. *Comput. Phys. Commun.* **1992**, *71*, 235.
(24) Liu, Y.-P.; Lynch, G. C.; Truong, T. N.; Lu, D.-h.; Truhlar, D. G.; Garrett, B. C. *J. Am. Chem. Soc.* **1993**, *115*, 2408.
(25) Garrett, B. C.; Joseph, T.; Truong, T. N.; Truhlar, D. G. *Chem. Phys.* **1989**, *136*, 271. Errata: **1990**, *140*, 207.
(26) Truong, T. N.; Lu, D.-h.; Lynch, G. C.; Liu, Y.-P.; Melissas, V. S.; Stewart, J. J. P.; Steckler, R.; Garrett, B. C.; Isaacson, A. D.; Gonzalez-Lafont, A.; Rai, S. N.; Hancock, G. C.; Joseph, T.; Truhlar, D. G. *Comput. Phys. Commun.* **1993**, *75*, 143.

(27) Liu, Y.-P.; Lu, D.-h.; Gonzalez-Lafont, A.; Truhlar, D. G.; Garrett, B. C. *J. Am. Chem. Soc*. **1993**, *115*, 7806.
(28) Truhlar, D. G. *J. Chem. Soc., Faraday Trans*. **1994**, *90*, 1740.
(29) Garrett, B. C.; Truhlar, D. G. *J. Chem. Phys*. **1983**, *79*, 4931.
(30) Garrett, B. C.; Truhlar, D. G.; Schatz, G. C. *J. Am. Chem. Soc*. **1986**, *108*, 2876.
(31) Mielke, S. L.; Allison, T. C.; Truhlar, D. G.; Schwenke, D. W. *J. Phys. Chem*. **1996**, *100*, 13588.
(32) Truhlar, D. G.; Brown, F. B.; Steckler, R.; Isaacson, A. D. In *The Theory of Chemical Reaction Dynamics*; Clary, D. C., Ed.; Reidel: Dordrecht, The Netherlands, 1986; pp 285−329.
(33) Truhlar, D. G.; Gordon, M. S. *Science* **1990**, *249*, 491.
(34) Eckart, C. *Phys. Rev*. **1930**, *35*, 1303.
(35) Dunning, T. H., Jr. *J. Chem. Phys*. **1989**, *90*, 1007.
(36) Hu, W.-P.; Lynch, G. C.; Liu, Y.-P.; Rossi, I.; Stewart, J. J. P.; Steckler, R.; Garrett, B. C.; Isaacson, A. D.; Lu, D.-h.; Melissas, V. S.; Truhlar, D. G. *QCPE Bull*. **1995**, *15*, 26.
(37) Stewart, J. J. P. *J. Comput.-Aided Mol. Des*. **1990**, *4*, 1.
(38) Baker, J.; Jensen, F.; Rzepa, H. S.; Stebbings, A. Location of Transition States in AMPAC and MOPAC Using Eigenvector Following (EF): Program 597. *QCPE Bull*. **1990**, *10*, 91.
(39) Page, M.; McIver, J. W., Jr. *J. Chem. Phys*. **1988**, *88*, 922.
(40) Pople, J. A.; Curtiss, L. A. *J. Chem. Phys*. **1991**, *95*, 4385.
(41) Gonzàlez-Lafont, A.; Truong, T. N.; Truhlar, D. G. *J. Chem. Phys*. **1991**, *95*, 8875.
(42) Jackels, C. F.; Gu, Z.; Truhlar, D. G. *J. Chem. Phys*. **1995**, *102*, 3188.
(43) Nguyen, K. A.; Jackels, C. F.; Truhlar, D. G. *J. Chem. Phys*. **1996**, *104*, 6491.
(44) Isaacson, A. D.; Truhlar, D. G. *J. Chem. Phys*. **1982**, *76*, 1380.
(45) Truhlar, D. G. *J. Comput. Chem*. **1991**, *12*, 266.
(46) Truhlar, D. G.; Isaacson, A. D. *J. Chem. Phys*. **1991**, *94*, 2040.
(47) Kuhler, K. M.; Truhlar, D. G.; Isaacson, A. D. *J. Chem. Phys*. **1996**, *104*, 4664.